Proc. Natl. Acad. Sci. USA
Vol. 94, pp. 8411–8416, August 1997
Biochemistry

Three-dimensional structure of NADPH–cytochrome P450 reductase: Prototype for FMN- and FAD-containing enzymes

(x-ray crystallography/flavoprotein/nitric-oxide synthase)

MING WANG*, DAVID L. ROBERTS*, ROSEMARY PASCHKE*, THOMAS M. SHEA†, BETTIE SUE SILER MASTERS†, AND JUNG-JA P. KIM*‡

*Department of Biochemistry, Medical College of Wisconsin, Milwaukee, WI 53226; and †Department of Biochemistry, University of Texas Health Science Center at San Antonio, San Antonio, TX 78284

Communicated by Ronald W. Estabrook, University of Texas Southwestern Medical Center, Dallas, TX, May 30, 1997 (received for review May 7, 1997)

ABSTRACT **Microsomal NADPH–cytochrome P450 reductase (CPR) is one of only two mammalian enzymes known to contain both FAD and FMN, the other being nitric-oxide synthase. CPR is a membrane-bound protein and catalyzes electron transfer from NADPH to all known microsomal cytochromes P450. The structure of rat liver CPR, expressed in *Escherichia coli* and solubilized by limited trypsinolysis, has been determined by x-ray crystallography at 2.6 Å resolution. The molecule is composed of four structural domains: (from the N- to C- termini) the FMN-binding domain, the connecting domain, and the FAD- and NADPH-binding domains. The FMN-binding domain is similar to the structure of flavodoxin, whereas the two C-terminal dinucleotide-binding domains are similar to those of ferredoxin–NADP$^+$ reductase (FNR). The connecting domain, situated between the FMN-binding and FNR-like domains, is responsible for the relative orientation of the other domains, ensuring the proper alignment of the two flavins necessary for efficient electron transfer. The two flavin isoalloxazine rings are juxtaposed, with the closest distance between them being about 4 Å. The bowl-shaped surface near the FMN-binding site is likely the docking site of cytochrome *c* and the physiological redox partners, including cytochromes P450 and *b*5 and heme oxygenase.**

Cytochrome P450-mediated microsomal electron transport is responsible for oxidative metabolism of both endogenous compounds, including fatty acids, steroids, and prostaglandins, and exogenous compounds ranging from therapeutic drugs and environmental toxicants to carcinogens. It is mediated by a multicomponent monooxygenase system, in which reducing equivalents from NADPH ultimately are transferred to molecular oxygen (for review, see refs. 1 and 2). In its simplest form, the monooxygenase system consists of NADPH-cytochrome P450 reductase (CPR; NADPH–ferrihemoprotein reductase, EC 1.6.2.4) and one of many cytochrome P450 isozymes (3, 4). Both CPR and microsomal cytochromes P450 are integral membrane proteins, and CPR is one of only two known mammalian enzymes containing both FMN and FAD as prosthetic groups, the other being various isoforms of nitric-oxide synthase (NOS). Other physiological electron acceptors of CPR include microsomal heme oxygenase (5) and cytochrome *b*5 (6) and, although nonphysiological, CPR is capable of transferring reducing equivalents to cytochrome *c* (7). By virtue of the fact that only two protein components are required to catalyze the hydroxylation of a number of substrates, this system represents a simple model for other, more complex electron transport systems.

CPR accepts a pair of electrons from NADPH as a hydride ion, with FAD and FMN being the port of entry and exit, respectively, and transfers these electrons one at a time to cytochromes P450. Cytochromes P450, in turn, use these reducing equivalents for the hydroxylation of a variety of substrates. The redox potentials of each flavin half-reaction in the native enzyme have been determined by potentiometric titrations (8, 9). The enzyme cycles between $1e^-$ and $3e^-$ reduced levels (or $2e^-$ and $4e^-$), with the one-electron-reduced semiquinone of the FMN being the highest oxidation state during catalytic turnover (10, 11).

Amino acid sequences for several CPRs from different species ranging from yeast to trout to human reveal high sequence homology, indicating the importance of the enzyme throughout the course of evolution (1). The enzyme has two functional domains, a hydrophobic N-terminal membrane-binding domain and a hydrophilic C-terminal catalytic domain that is comprised of several structural domains. The hydrophobic N-terminal domain (6 kDa) serves to anchor the protein molecule to the endoplasmic reticulum and nuclear envelope (12), thus ensuring proper spatial interaction for electron transfer between the reductase and cytochromes P450. The membrane-bound CPR can be solubilized by limited proteolysis with pancreatic steapsin or trypsin, releasing the C-terminal hydrophilic 72-kDa domain. Without the hydrophobic anchor, the larger soluble domain is still capable of passing electrons to cytochrome *c* and other artificial electron acceptors, but is incapable of transferring electrons to cytochromes P450. Amino acid sequence analysis predicted that this anchor-less C-terminal hydrophilic domain can be further divided into two structural domains. The N-terminal domain, consisting of approximately 170 amino acid residues, is homologous to that of the bacterial flavodoxin, suggesting that this portion of the reductase is likely to bind FMN, and the C-terminal region contains segments with considerable sequence similarity to two NAD(P)H dependent FAD-containing enzymes, ferredoxin–NADP$^+$ reductase (FNR), and NADH–cytochrome *b*5 reductase, indicating that this portion binds FAD and NADPH (13). This distinct domain arrangement is consistent with results from further studies in which each domain was expressed independently (14), and unfolding of the polypeptide was correlated with the release of each individual flavin (15). CPR has been studied extensively by a number of biophysical methods, including EPR spectroscopy (16, 17), time-resolved fluorescence spectroscopy (18, 19), ^{31}P NMR (20, 21), and resonance Raman spectroscopy

The publication costs of this article were defrayed in part by page charge payment. This article must therefore be hereby marked "*advertisement*" in accordance with 18 U.S.C. §1734 solely to indicate this fact.

Abbreviations: CPR, NADPH–cytochrome P450 reductase; FNR, ferredoxin-NADP$^+$ reductase; NOS, nitric-oxide synthase.

Data deposition: The atomic coordinates have been deposited in the Brookhaven Protein Data Bank, Upton, NY 11973 (ID code, 1amo).

‡To whom reprint requests should be addressed at: Department of Biochemistry, Medical College of Wisconsin, 8701 West Watertown Plank Road, Milwaukee, WI 53226. e-mail: jjkim@post.its.mcw.edu.

Table 1. Data collection statistics

Data set	Native	K_2OsCl_6	$PtCl_4$	K_2OsCl_6 + K_2PtCl_6	Thimerosal
Resolution, Å*	2.6 (2.76-2.6)	3.0 (3.25-3.0)	3.0 (3.25-3.0)	3.0 (3.23-3.0)	2.8 (3.23-3.0)
Unique reflections	41,132	26,064	27,320	20,104	26,599
Total observations	171,499	128,475	152,158	120,324	113,336
Completeness, %	91.5 (85.8)	87.6 (78.8)	91.7 (85.7)	68.1 (42.0)	89.1 (85.5)
R_{sym}, %†	7.0 (30.8)	6.4 (20.4)	6.2 (17.3)	5.8 (22.7)	8.6 (25.2)
R_{iso}, %‡	—	13.5	12.4	15.3	17.0
Soaking conditions	—	1 mM/36 hr	1 mM/18 hr	1 mM/4 hr + 1 mM/20 hr	3 mM/72 hr
Number of sites	—	2	4	6	4
Phasing power, 3 Å§	—	1.67 [0.80]	1.09 [0.93]	1.32 [0.60]	1.14 [0.83]
R_{cullis}	—	0.666	0.670	0.676	0.689
Mean figure of merit	0.596	0.352 [0.194]	0.222 [0.218]	0.274 [0.123]	0.237 [0.193]

The final crystallographic *R*-factor was 20.0% with *R*-free of 31.0% for a total of 10,156 nonhydrogen atoms, including 78 solvent atoms.
*Highest resolution shell statistics are given in parenthesis; statistics for anomalous data sets are shown in brackets.
†$R_{sym} = \Sigma_h\Sigma_i|I_{hi} - \langle I_h\rangle|/\Sigma_h\Sigma_i|I_{hi}|$, where h are unique reflection indices and i indicate symmetry equivalent indices.
‡$R_{iso} = \Sigma||I_{ph}| - |I_p||/\Sigma|I_p|$ for isomorphous replacement data.
§Phasing power = f_{rms}/E_{rms}, where $f_{rms} = [(\Sigma f_h^2)/n]^{1/2}$ and $E_{rms} = [\Sigma(F_{ph} - |F_p + f_h|)^2/n]^{1/2}$.

(22). Despite these intensive studies, little has been determined about physical and electronic interactions between FMN, FAD, and NADPH and interactions between CPR and its electron transfer partners. We now describe the complete three-dimensional structure of rat liver CPR expressed in *Escherichia coli* and treated by limited trypsinolysis. The structure represents a prototype for the spatial arrangements of the two flavins in the enzyme and provides insights into not only the interactions of CPR with its physiological electron acceptors, including cytochromes P450, but also the mechanism of electron-transfer and its regulation in other FMN- and FAD-containing enzymes, including NOSs.

Purification and Crystallization of CPR. Rat liver CPR was cloned in *E. coli* and purified as described (23). Purification of the full-length CPR protein involved centrifugation, solubilization using Triton X-100, ultracentrifugation, and finally affinity chromatography on a 2′,5′-ADP Sepharose 4B affinity column in the presence of Triton X-100. The holo CPR was treated with immobilized trypsin, and the clipped CPR (hereafter referred to simply as CPR) was further purified in the absence of any detergent. Final purification of the clipped enzyme required hydroxyapatite chromatography using a Bio-Rad ceramic FPLC column.

The purified CPR was crystallized as previously described (24). Crystallization of CPR required adding excess FMN and $NADP^+$ during the concentration/dilution procedure, and any excess cofactors were removed before setting up the crystallization trials. Crystals were obtained by the vapor diffusion method; the final crystallization involved mixing equal volumes of CPR (25 mg/ml) and precipitant (21% PEG 4500/150 mM Hepes, pH 6.5/5 mM $MgCl_2$/0.8 M NaCl), and equilibrating against precipitant at 19°C. Crystals routinely grew to approximately 0.3 mm × 0.5 mm × 0.6 mm within 2–3 weeks. Data collection was performed on an R-AXIS II image plate system at 4°C. The CPR crystals belong to the orthorhombic space group $P2_12_12_1$, with unit cell parameters a = 103.28 Å, b = 116.18 Å, and c = 119.77 Å. Assuming two molecules per asymmetric unit, the calculated V_m value is 2.49 Å^3/Da (25).

Structure Determination of CPR. The structure was solved using multiple isomorphous replacement methods together with anomalous scattering data. Self-rotation function analysis was not successful, but self-Patterson analysis revealed a large peak around (u, v, w)= (1.0, 0.22, 0.5), indicating that the local 2-fold axis is parallel to the *z*-axis, located near (x, y) = (0.25, 0.11). During heavy atom screening, the degree of isomorphism between the native data set and the derivative data sets was monitored by following the position of the self-Patterson peak. If the peak position varied by more than 3%, it was not considered isomorphous to the native data and was not used for phasing analysis. This nonisomorphism was not necessarily a result of the derivative soaking, because oftentimes two different native crystals showed the same trend in nonisomorphism. Four isomorphous derivatives were obtained that were suitable for obtaining the initial phases (Table 1). The positions and occupancies of the heavy atoms were initially refined using the program HEAVY (26), and multiple isomorphous replacement phases were calculated and refined using the PHASES package (27). Initial electron density maps were calculated using data between 30 and 3.0 Å resolution. The phases were further improved by density modification

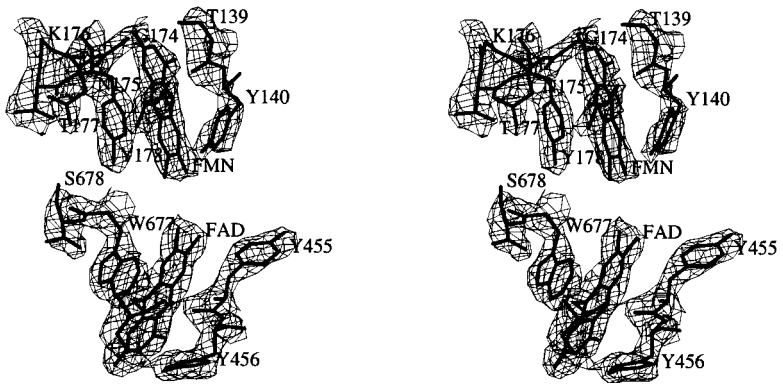

FIG. 1. Stereoview of the electron density in the vicinity of the FAD and FMN of CPR. The $3|F_o| - 2|F_c|$ electron density map computed with 2.6 Å resolution data is contoured at 1.2σ level. Residues within close contact of the flavin ring are labeled. Four aromatic residues sandwich the flavin rings: Y178 and Y140 for FMN and Y456 and W677 for FAD.

using the solvent flattening procedure, as well as noncrystallographic symmetry averaging (28). At this time, well defined α-helices and β-strands were easily identified. A polyalanine model was then constructed using the molecular graphics program TURBO-FRODO (29) on a silicon graphics workstation.

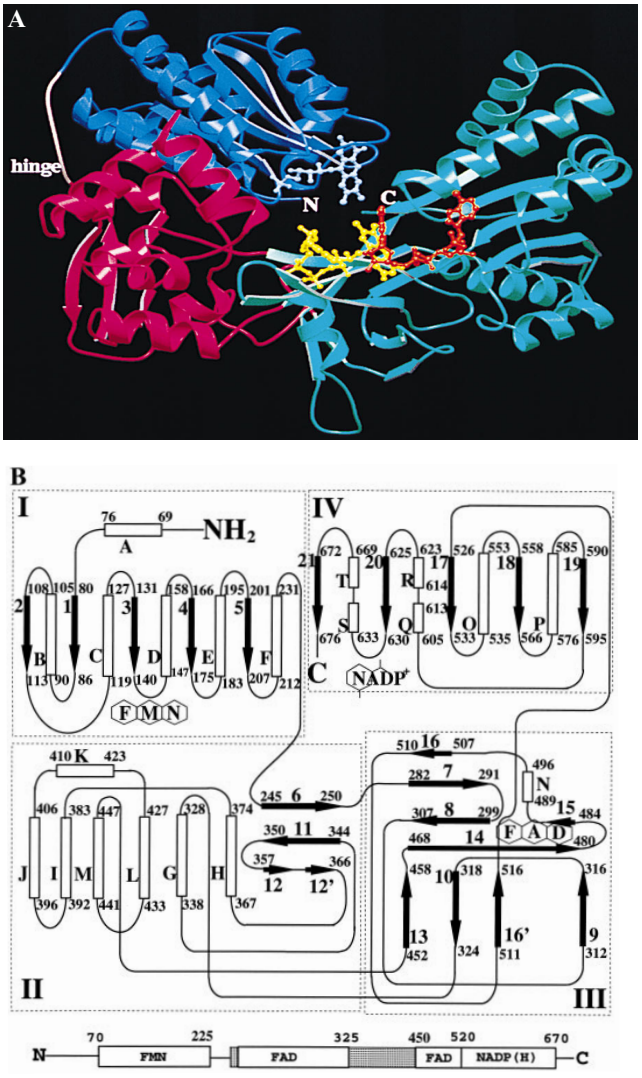

FIG. 2. Overall polypeptide fold and topology diagram for CPR. (*A*) Ribbon diagram showing the structure of CPR. The FMN-binding domain is shown in blue, the connecting domain in red, and the FAD- and NADP(H)-domains are represented in green. The cofactors are shown as ball and sticks, with the FMN (light blue), FAD (yellow), and $NADP^+$ (orange). A disordered region that represents a "hinge" is shown in pink (between the FMN-binding and the connecting domain). The drawing was generated using MOLSCRIPT (32) and RASTER3D (33). (*B*) Topology diagram of the CPR protein, indicating regions responsible for cofactor recognition. α-Helices (open cylinders), β-strands (filled arrows), random coils (lines), and corresponding residue numbers are indicated. The FMN domain (I), connecting domain (II), FAD domain (III), and $NADP^+$ domain (IV) are identified by boxes. Domains II and III are not contiguous in linear sequence, and the last two nucleotide binding domains (III and IV) form an FNR-like structure. The α-helices are lettered, and the β-strands are numbered sequentially from N to C termini. A linear diagram showing domain arrangement in the CPR structure is shown at the bottom. Each cofactor binding domain is indicated, and the connecting domain is depicted as stippled boxes. The numbers above the boxes indicate approximate amino acid positions for the corresponding domains in the CPR structure. The connecting domain and the FAD-binding domain are intertwined in linear sequence, yet both of them make distinctive structural domains.

The location of the FAD and FMN cofactors was easily identified (Fig. 1), and the structures of flavodoxin and FNR were superimposed onto the CPR density, aiding in chain-tracing. After building the initial model of CPR, electron density maps were generated by combining the multiple isomorphous replacement phases and those of the model according to the SIGMAA algorithm (30). Phase combination allowed for completion of the chain tracing. After several cycles of manually adjusting the model to fit the electron density maps, along with additional sequence assignment followed by refinement using the X-PLOR package (31), the entire sequence was assigned. The polypeptide connectivity was confirmed by calculating simulated annealing omit maps. The first seven residues (residues 57 to 63) at the N terminus and 10 residues in the hinge region (residues 234 to 243) are disordered in the refined structure. The final *R*-factor was 20.0%, with an R_{free} of 31.0%, including 78 water molecules, for 37,048 reflections between 10 and 2.6 Å resolution with $I/\sigma > 2.0$. The rms deviations of the bond lengths and bond angles of the final structure are 0.007 Å and 1.5°, respectively.

The Overall Structure and Domain Organization. Sequence analysis of dissolved crystalline protein revealed that the N terminus residue is Ile-57. The structure, however, as seen in the crystallographic electron density map, begins with Val-64 indicating that the N terminus of the hydrophilic domain of CPR is flexible. This is consistent with biochemical studies indicating that this region is highly exposed in the intact enzyme and is very susceptible to proteolytic cleavage, as well as crystallographic studies in which we failed to crystallize the intact CPR protein, due to persistent cleavage at this region. An overview of the backbone structure of CPR in ribbon representation and its topology diagram are shown in Fig. 2. The structure of CPR is composed of four structural domains. From N to C terminus, they are the FMN-binding domain, the connecting domain, and the FAD- and the NADP-binding domains, consistent with the previous prediction from the sequence alignment (13). Similar to the flavodoxin structure from *Desulfovibrio vulgaris* (34), the FMN binding domain consists of a five-stranded parallel β-sheet flanked by five α-helices (Fig. 2*B*) with the FMN positioned at the tip of the C-terminal side of the β-sheet. As seen in the structures of FNR (35) and other FNR-like enzymes such as cytochrome *b*5 reductase (36) and corn nitrate reductase (37), the core of the FAD-binding domain is an anti-parallel flattened β-barrel, and that of the NADP(H)-binding domain is another parallel five-stranded β-sheet sandwiched by α-helices. The connecting domain, situated between the two flavin domains, consists of residues between 240 to 270 and between 325 to 450 and is comprised mainly of α-helices. This domain appears to be responsible for bringing the two flavins together and, there-

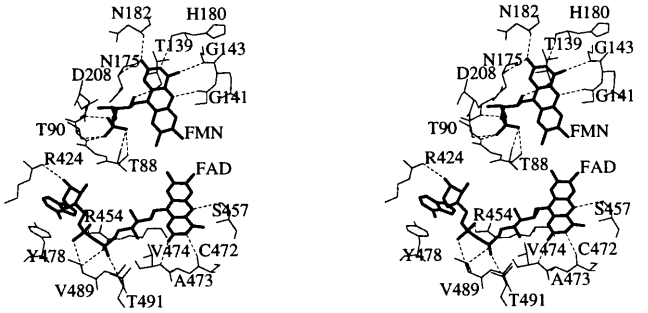

FIG. 3. Stereoview showing residues in the vicinity of the FAD and FMN cofactors. The FAD and FMN cofactors in CPR are oriented such that the xylene portions of both isoalloxazine rings are pointed toward each other. The FAD is in an extended conformation. Potential hydrogen bonds are indicated by dotted lines. For clarity, the aromatic residues sandwiching both isoalloxazine rings shown in Fig. 1 are not drawn in this figure.

fore, for modulating electron transfer between the two flavins. The loop between helix F and strand 6 is not well ordered in the crystal structure (Fig. 2*A*) and forms a hinge between the FMN-binding domain and the connecting domain (Fig. 2*B*). Residues located at the interface between the FMN binding- and the connecting-domains are mainly hydrophilic, and, therefore, the interaction between them is largely electrostatic. The location of FMN in the FMN-binding domain and movement of this domain that exposes the FMN to solvent are consistent with previous biochemical findings that describe the ease with which FMN dissociates from the enzyme (9, 15), as movement of this domain would coincide with FMN release/binding. On the other hand, the interfaces between the connecting domain and the FAD-binding domain, and between the FAD- and the NADP(H)-binding domains are relatively hydrophobic, again explaining the sequential release of FAD only after protein unfolding upon treatment with chaotropes. Furthermore, the linear sequence for the latter three domains are intertwined, and therefore these domains may not be functionally separable. The overall shape of the molecule as viewed in Fig. 2*A* is an oval-shaped bowl that is approximately 50 Å deep × 70 Å wide × 60 Å high, and the cofactors lie in the middle of the bowl.

FMN- and FAD-Binding Sites. FMN is located at the C-terminal side of the β-strands in the FMN-binding domain (Fig. 2*A*). As seen in Figs. 1 and 3, the two flavins do not overlie each other, but rather are end on and communicate with each other through the 7- and 8-methyl groups of the xylene rings. The two isoalloxazine rings make an angle of about 150° to each other, forming an almost continuous "ribbon" with the closest distance between them being 3.5 Å between the C_7M atoms and 4.5 Å between the C_8M atoms of the xylene rings. This arrangement indicates that the electron flow between the two flavins is not mediated by any amino acid residue atoms, and instead is direct, consistent with kinetic data indicating that the electron transfer between the two flavins is rapid. Both ends of the flavin ribbon are made up of the pyrimidine side of the isoalloxazine ring and are hydrogen bonded to the main chain atoms of the polypeptide (Fig. 3). FMN lies at the C-terminal tip of the β-sheet in the FMN-binding domain and is bound to polypeptide fragments ^{139}TYGEGPD and ^{175}NKTYEHFN, and the FAD is encompassed by fragments ^{455}YYSIAS and ^{471}ICAVAV. The isoalloxazine ring of FMN is covered by the phenolic ring of Y140 at the re-side and Y178 at the si-side (Fig. 1). As observed in the FNR structure (35), the FAD is bound in an extended conformation, and the isoalloxazine ring is inserted at the boundary between the FAD- and the NADP(H)-binding domains, whereas the rest of the FAD molecule lies at the interface between the FAD-binding domain and the connecting domain. The re-side of the FAD ring is stacked with the indole ring of W677 and Y456 lies at its si-side (Fig. 1). As in the FNR structure, the pyrophosphate is stabilized by side chains from T491 and R454, and the polypeptide segment of residues C472 to Y478 is almost parallel to the ribityl-pyrophosphate chain. The adenosine moiety is rather exposed, and the phenolic ring of Y478 is stacking on one side of the adenine ring (Fig. 3).

$NADP^+$ Adopts Multiple Conformations. The electron density for the ribose-nicotinamide moiety of the bound $NADP^+$ is only about 30% of that of the rest of the molecule in both molecules of the asymmetric unit. Furthermore, its conformation is different in the two structures, indicating that this portion of the molecule is highly flexible and disordered. Although the exact conformation of the ribose-nicotinamide moiety cannot be defined from current data, an approximate model can be built in each structure, only to be used to estimate the relative orientation of the bound $NADP^+$ with respect to the FMN and FAD (Fig. 4). The two observed conformations are easily interconvertible by changing the dihedral angle by about 120° of the nicotinamide side of the pyrophosphate (—P_N—O—P_A—) bond. However, in both conformations, the distance between the C4 atom of the nicotinamide (the hydride donor) and the N5 of the FAD isoalloxazine ring (the hydride acceptor) is over 9 Å in one and over 14 Å in the other conformer, indicating that neither of these conformations of $NADP^+$ is capable of direct hydride transfer to FAD. Therefore, the enzyme-$NADP^+$ complex structure observed in both crystal forms must represent the enzyme-product complex of the reductive half reaction. It should be noted that, by changing the dihedral angles of both sides of the bridging pyrophosphate oxygen atom (—P_N—O—P_A—) of the $NADP^+$ molecule, the nicotinamide ring could be positioned at the re-side of the FAD ring where W677 lies (Fig. 4), in a manner similar to that observed in the glutathione reductase structure and to that suggested by Karplus *et al.* (35) for the FNR structure. In the case of glutathione reductase, the phenolic ring of Y197 covers the si-face of the FAD ring in the oxidized state, but flips away to make room for the nicotinamide ring of the NADPH when it binds to the enzyme to form a reduced enzyme-NADPH complex (38). Despite numerous attempts, no crystal structure is available of an FNR family member showing nicotinamide nucleoside conformation in an enzyme-NAD(P)(H) complex. No electron density was observed for the nicotinamide nucleoside moiety in the crystal structure of the reduced FNR-NADPH complex (39). Interestingly, similar results were observed in the studies of phthalate dioxygenase reductase (40), a member of an extended FNR family in which a

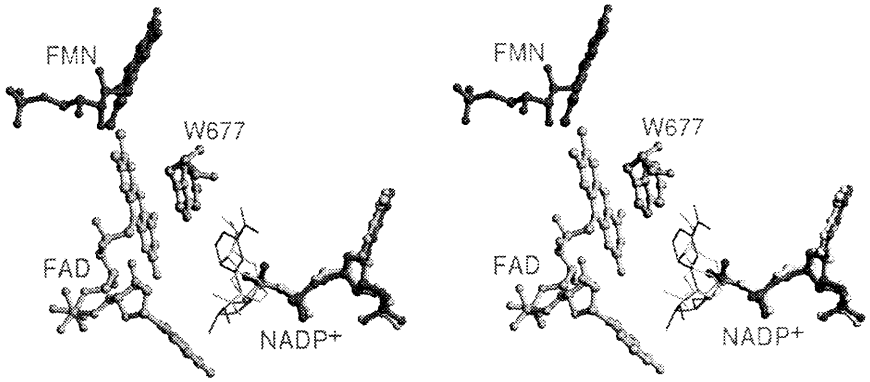

FIG. 4. Stereoview of the cofactor arrangement in CPR and multiple conformers for the bound $NADP^+$. Electrons flow from NADPH to FAD and then to FMN. The FMN and FAD are represented by ball-and-stick, with the xylene portions of the isoalloxazine rings oriented toward each other. The adenine portion of $NADP^+$ binds in a single conformation (ball-and-stick) while the nicotinamide (stick only) binds in multiple conformations. By rotation about the P_N—O—P_A bond, the nicotinamide ring could displace W677 at the re-side of the FAD ring, placing it in the optimum orientation for hydride transfer from the NADPH to the N5 position of the FAD cofactor.

ferredoxin-like [2Fe–2S] domain is attached to the C terminus of an FNR-like module.

Interactions with Cytochrome *c* and Cytochromes P450. As the soluble form of CPR is capable of transferring electrons from NADPH to cytochrome *c*, we attempted to map out the cytochrome *c* binding surface of the CPR molecule. Because the pyrimidine side of the FMN isoalloxazine ring lies close to the solvent accessible surface of the CPR molecule, it is reasonable to assume that electrons must exit from this side of the FMN through the FMN-binding domain and enter the heme of the acceptor molecule. Thus, the FMN-binding domain must provide a major portion of the docking surface. This is further supported by the fact that bacterial flavodoxin can serve to transfer electrons to cytochromes P450, either combined with the NADPH-reduced flavodoxin reductase (41) or when electrochemically reduced using dye (42). Fig. 5*A* shows a plausible mode of docking between cytochrome *c* and CPR that minimizes the distance between the two redox centers (FMN and the heme) and allows a maximum contact area between the two molecules. It also allows a positively charged cytochrome *c* surface to bind to the mostly negatively charged CPR surface. The model was obtained by manual inspection of two structures, followed by rigid body energy minimization using the X-PLOR package. The closest distance between the FMN of CPR and the heme of cytochrome *c* is less than 9 Å. The electrostatic potential mapped onto the docking surfaces of CPR and cytochrome *c* molecules are shown (Fig. 5*B*). The CPR docking surface contains the loop between strand 4 and helix E, consisting of residues 175 to 182, and the loop between strand 5 and helix F, containing residues 207 to 211 (Fig. 2*B*). The latter loop contains the acidic residues that were indicated to be involved in the binding of CPR to cytochrome *c* and cytochromes P450 by chemical crosslinking (45) and site-directed mutagenesis studies (46). This surface is, most likely, a major portion of the cytochromes P450 binding surface as evidenced by the inhibition of cytochromes P450 reactions by cytochrome *c* (47). A large portion of this surface also would overlap with the cytochrome *b*5 binding surface. Because cytochromes P450 are larger molecules than cytochromes *c* or *b*5, the contact surface with CPR would be larger, therefore, the CPR "bowl" would be filled to its rim with the P450 molecule. Furthermore, for the membrane-bound electron transfer partners, hydrophobic interactions between the membrane domains of the intact CPR and cytochromes P450 (or cytochrome *b*5) must play a significant role in addition to the ionic interactions described above.

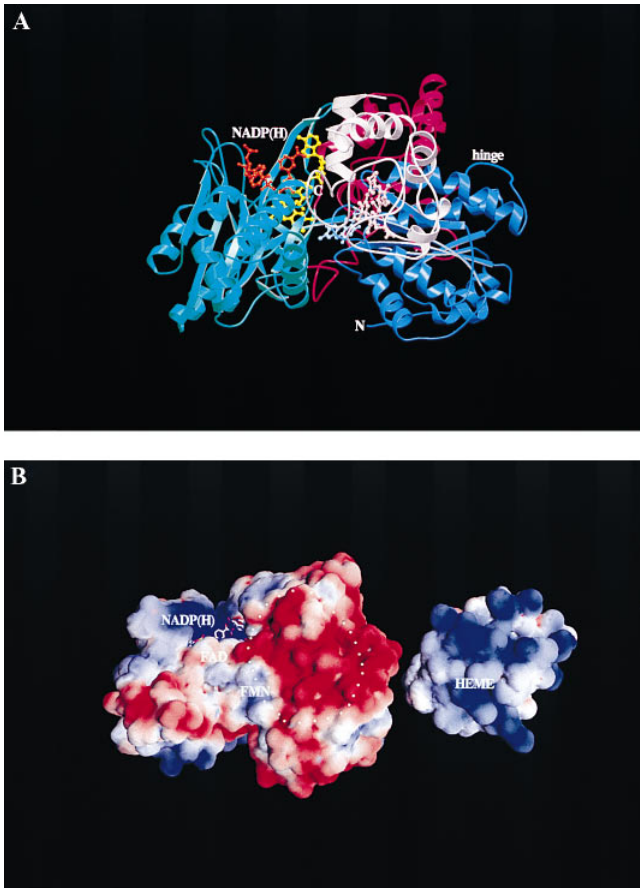

FIG. 5. Putative docking surface of CPR with its electron transfer partners. (*A*) Ribbon diagram showing the putative docking of CPR and cytochrome *c* in an orientation that represents CPR "sitting" on the membrane surface. The N-terminal membrane anchor portion of CPR, which was proteolytically removed for crystallization studies, would protrude downwards, into the membrane. Cytochrome *c* (or cytochrome P450) binds "in front of" the CPR molecule, allowing the NADP(H) to enter/exit freely from above, while the FMN and FAD are buried in the complex. The domains and cofactors of CPR are colored as shown in Fig. 2*A*, and cytochrome *c* is in pink. Because the cytochrome P450 is membrane-bound, interactions between the membrane domains of the two proteins would be possible in this "side-by-side" orientation. (*B*) The electrostatic potential mapped onto the solvent accessible surface of CPR (*Left*) and cytochrome *c* (*Right*). The view for CPR is the same as in *A*. The positive potential is shown in blue, and the negative potential is shown in red. The potential was calculated with Delphi (43) using formal charges and contoured at 2.5 *kT*, and mapped onto the solvent-accessible surface using GRASP (44). From this view, it is clear that the interactions between CPR and cytochrome *c* are primarily electrostatic in nature. The putative surface of CPR onto which cytochrome *c* binds is indicated with a dotted circle.

Membrane-Binding Site. The N terminus of the CPR molecule is situated at the opposite side of the $NADP^+$ binding site (back side of the molecule shown in Fig. 2*A*). The membrane-binding site of the CPR structure is likely to be situated around Val-64 and near some hydrophobic patches of the CPR surface, most likely, containing loops 516–525, 250–281, and 553–557. Fig. 5*A* illustrates the orientation of a CPR molecule "sitting" on the membrane surface. The NADP(H) molecule is bound on the cytoplasmic side of the molecule, and the N terminus is facing to the membrane side. In this view, cytochrome *c* or other electron transfer partners would bind "in front of" the molecule where it can communicate with the FMN most directly. This "side-by-side" orientation of P450 and CPR would make it simpler for the two membrane-bound molecules to interact on the membrane.

The CPR Family. CPR belongs to a family of enzymes that contain both FMN and FAD and shuttles electrons between pyridine nucleotide and heme via FAD and FMN. In addition to CPR, the family includes P450BM-3, NOS, and bacterial sulfite reductase. It is a subfamily of the FNR superfamily, a structurally designated family of proteins whose common feature is an FNR-like domain (48). Amino acid sequence analysis of the CPR family members reveals striking similarities among them, ranging from 50% between CPR and the α-subunit of sulfite reductase to 58% between CPR and the C-terminal 640 residues of neuronal NOS (49). A sequence alignment for the cofactor-binding regions of the flavin domains of P450-BM3, rat neuronal NOS, and the α-subunit of *E. coli* sulfite reductase, along with CPR, is shown in Fig. 6. In addition, using structural alignment, the N-terminal FMN-binding domain was aligned with flavodoxin, whereas the C-terminal portion was aligned with the FNR structure. Sequences for most of the secondary structural elements are conserved, as well as all cofactor binding sites, indicating that the polypeptide folding and the cofactor arrangement in the structures of other members of the CPR family are very similar to those of CPR. Thus, the structure of CPR can serve as a model for understanding the mechanism and function of the other members of the CPR family. Furthermore, it provides a

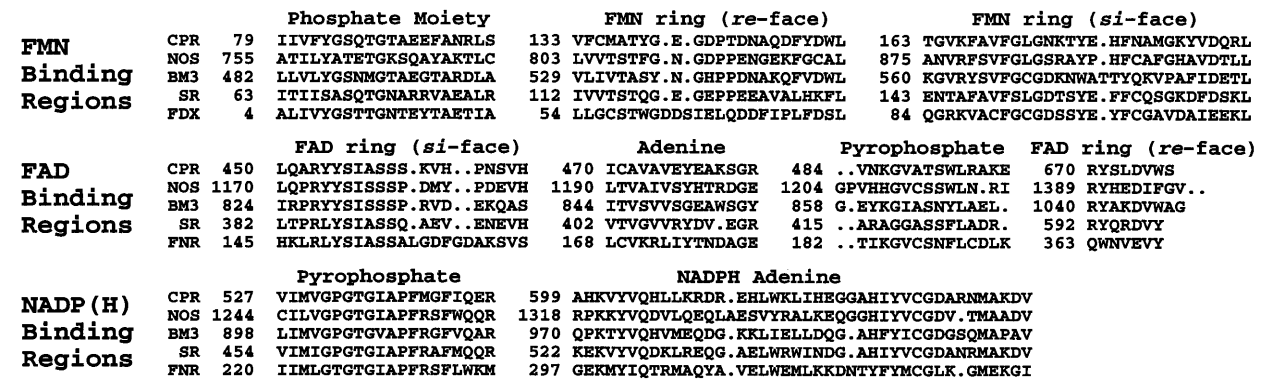

FIG. 6. Sequence lineup for cofactor-binding regions of key members of the CPR family. The proteins represented in the lineup are: CPR, rat cytochrome P450 reductase; NOS, rat neuronal nitric-oxide synthase; BM3, cytochrome P450 BM-3; SR, *E. coli* sulfite reductase; FDX, *D. vulgaris* flavodoxin; and FNR, *Spinacia oleracea* FNR. The numbering is for the first amino acid of each region for the given protein. The lineups of FDX and FNR were made by superimposing the molecular structures onto the CPR structure.

model for studying not only flavin–flavin interactions, but also electron transfer mechanisms among flavoproteins, in general.

We thank J. P. Fulmer for making Fig. 5*B*. This work was supported by Grants GM52682 (J.-J.P.K.) and HL30050 (B.S.S.M.) from the National Institutes of Health.

1. Shen, A. L. & Kasper, C. B. (1993) in *Handbook of Experimental Pharmacology*, eds. Schenkman, J. B. & Greim, H. (Springer, New York), pp. 35–59.
2. Strobel, H. W., Hodgson, A. V., & Shen, S. (1995) in *Cytochrome P450: Structure, Mechanism, and Biochemistry*, ed. Ortiz de Montellano, P. R. (Plenum, New York), pp. 225–244.
3. Williams, C. H. & Kamin, H. (1962) *J. Biol. Chem.* **237,** 587–595.
4. Phillips, A. H. & Langdon, R. G. (1962) *J. Biol. Chem.* **237,** 2652–2660.
5. Schacter, B. A., Nelson, E. B., Marver, H. S. & Masters, B. S. S. (1972) *J. Biol. Chem.* **247,** 3601–3607.
6. Enoch, H. G. & Strittmatter, P. (1979) *J. Biol. Chem.* **254,** 8976–8981.
7. Horecker, B. L. (1950) *J. Biol. Chem.* **183,** 593–605.
8. Iyanagi, T., Makino, N. & Mason, H. S. (1974) *Biochemistry* **13,** 1701–1710.
9. Vermilion, J. L. & Coon, M. J. (1978) *J. Biol. Chem.* **253,** 8812–8819.
10. Masters, B. S. S., Bilimoria, M. H. & Kamin, H. (1965) *J. Biol. Chem.* **240,** 4081–4088.
11. Backes, W. L. & Reker-Backes, C. E. (1988) *J. Biol. Chem.* **263,** 247–253.
12. Kasper, C. B. (1971) *J. Biol. Chem.* **246,** 577–581.
13. Porter, T. D. & Kasper, C. B. (1986) *Biochemistry* **25,** 1682–1687.
14. Smith, G. C., Tew, D. G. & Wolf, C. R. (1994) *Proc. Natl. Acad. Sci. USA* **91,** 8710–8714.
15. Narayanasami, R., Horowitz, P. M. & Masters, B. S. S. (1995) *Arch. Biochem. Biophys.* **316,** 267–274.
16. Iyanagi, T. & Mason, H. S. (1973) *Biochemistry* **12,** 2297–2308.
17. Yasukochi, Y., Peterson, J. A. & Masters, B. S. S. (1979) *J. Biol. Chem.* **254,** 7097–7104.
18. Blumberg, W. E., Nisimoto, Y. & Mason, H. S. (1982) in *Oxygenases and Oxygen Metabolism*, eds. Nozake, M., Yamamoto, S., Ishimura, Y., Coon, M. J., Ernster, L. & Estabrook, R. W. (Academic, New York), pp. 333–343.
19. Bastiaens, P. I. H., Bonants, P. J. M., Müller, F. & Visser, A. J. (1989) *Biochemistry* **28,** 8416–8425.
20. Bonants, P. J., Müller, F., Vervoort, J. & Edmondson, D. E. (1990) *Eur. J. Biochem.* **190,** 531–537.
21. Narayanasami, R., Otvos, J. D., Kasper, C. B., Shen, A., Rajagopalan, J., McCabe, T. J., Okita, J. R., Hanahan, D. J. & Masters, B. S. S. (1992) *Biochemistry* **31,** 4210–4218.
22. Sugiyama, T., Nisimoto, Y., Mason, H. S. & Loehr, T. M. (1985) *Biochemistry* **24,** 3012–3019.
23. Shen, A. L., Porter, T. D., Wilson, T. E. & Kasper, C. B. (1989) *J. Biol. Chem.* **264,** 7584–7589.
24. Djordjevic, S., Roberts, D. L., Wang, M., Shea, T., Camitta, M. G. W., Masters, B. S. S. & Kim, J. J. P. (1995) *Proc. Natl. Acad. Sci. USA* **92,** 3214–3218.
25. Matthews, B. W. (1968) *J. Mol. Biol.* **33,** 491–497.
26. Terwilliger, T. C. & Eisenberg, D. (1983) *Acta Crystallogr. A* **39,** 813–817.
27. Furey, W. (1995) PHASES *Manual* (Veterans Administration Medical Center, Pittsburgh, PA).
28. Wang, B. C. (1985) *Methods Enzymol.* **115,** 90–112.
29. Cambillau, C. & Roussel, A. (1993) TURBO-FRODO: *Manual for a Molecular Graphics Program for Silicon Graphics* (Silicon Graphics, Mountain View, CA), Version 5.4.
30. Read, R. J. (1986) *Acta Cryst. A* **42,** 140–149.
31. Brunger, A. T. (1992) X-PLOR: *A System for X-ray Crystallography and NMR,* (Yale Univ. Press, New Haven, CT), Version 3.1.
32. Kraulis, P. J. (1991) *J. Appl. Crystallogr.* **24,** 946–950.
33. Merritt, E. A. & Murphy, M. E. P. (1994) *Acta. Crystallogr. D* **50,** 869–873.
34. Watenpaugh, D. K., Sieker, L. C. & Jensen, L. H. (1973) *Proc. Natl. Acad. Sci. USA* **70,** 3857–3860.
35. Karplus, P. A., Daniels, M. J. & Herriott, J. R. (1991) *Science* **251,** 60–66.
36. Nishida, H., Inaka, K., Yamanaka, M., Kaida, S., Kobayashi, K. & Miki, K. (1995) *Biochemistry* **34,** 2763–2767.
37. Lu, G., Lindqvist, Y., Schneider, G., Dwivedi, U. & Campbell, W. (1995) *J. Mol. Biol.* **248,** 931–948.
38. Pai, E. F., Karplus, P. A. & Schulz, G. E. (1988) *Biochemistry* **27,** 4465–4474.
39. Bruns, C. M. & Karplus, P. A. (1995) *J. Mol. Biol.* **247,** 125–145.
40. Correll, C. C., Batie, C. J., Ballou, D. P. & Ludwig, M. L. (1992) *Science* **258,** 1604–1610.
41. Jenkins, C. M. & Waterman, M. R. (1994) *J. Biol. Chem.* **269,** 27401–27408.
42. Estabrook, R. W., Shet, M. S., Fisher, C. W., Jenkins, C. M. & Waterman, M. R. (1996) *Arch. Biochem. Biophys.* **333,** 308–315.
43. Gilson, M. K., Rashin, A., Fine, R. & Honig, B. (1985) *J. Mol. Biol.* **183,** 503–516.
44. Nichols, A. (1992) GRASP: *Graphical Representation and Analysis of Surface Properties* (Columbia Univ., New York).
45. Nisimoto, Y. (1986) *J. Biol. Chem.* **261,** 14232–14239.
46. Shen, A. L. & Kasper, C. B. (1995) *J. Biol. Chem.* **270,** 27475–27480.
47. Gillette, J. R., Brodie, B. B. & La Du, B. N. (1957) *J. Pharmacol. Exp. Ther.* **119,** 532–541.
48. Andrews, S. C., Shipley, D., Keen, J. N., Findlay, J. B. C., Harrison, P. M. & Guest, J. R. (1992) *FEBS Lett.* **302,** 247–252.
49. Bredt, D. C., Hwang, P. M., Glatt, C. E., Lowenstein, C., Reed, R. R. & Snyder, S. H. (1991) *Nature (London)* **351,** 714–718.